Letter

Microscopic nature of the charge-density wave in the kagome superconductor RbV_3Sb_5

Jonathan Frassineti,[1] Pietro Bonfà,[2,*] Giuseppe Allodi,[2] Erick Garcia,[3] Rong Cong,[3] Brenden R. Ortiz,[4] Stephen D. Wilson,[4] Roberto De Renzi,[2] Vesna F. Mitrović,[3,†] and Samuele Sanna[1]

[1]*Department of Physics and Astronomy "A. Righi", University of Bologna and INFN Sezione di Bologna, via Berti Pichat 6/2, 40127 Bologna, Italy*

[2]*Department of Mathematical, Physical and Computer Sciences, University of Parma, Parco Area delle Scienze 7/A, 43124 Parma, Italy*

[3]*Department of Physics, Brown University, Providence, Rhode Island 02912, USA*

[4]*Materials Department and California Nanosystems Institute, University of California Santa Barbara, Santa Barbara, California 93106, USA*

(Received 20 October 2022; revised 21 December 2022; accepted 18 January 2023; published 10 February 2023)

The recently discovered vanadium-based Kagome metals AV_3Sb_5 (A = K, Rb, Cs) undergo a unique phase transition into charge-density wave (CDW) order which precedes both unconventional superconductivity and time-reversal symmetry breaking. Therefore the essential first step in building a full understanding of the role of CDW in establishing these unconventional phases is to unveil the symmetries and the microscopic nature of the charge-ordered phase. Here, we determine the exact structure of the $2 \times 2 \times 2$ superlattice that develops below the charge-density wave ordering temperature (T_{CDW}) in RbV_3Sb_5. We present a comprehensive set of ^{51}V, ^{87}Rb, and ^{121}Sb nuclear magnetic resonance (NMR) measurements and density functional theory simulations of NMR observables to provide a unique site-selective view into the local nature of the charge-ordered phase. The combination of these experimental results with simulations provides compelling evidence that the CDW structure prevailing below 103 K in RbV_3Sb_5 is the so-called inverse Star of David pattern, π-shifted along the c axis. These findings put severe constraints on the topology of these Kagome compounds and thus provide essential guidance for the development of an appropriate theoretical framework for predicting properties of exotic electronic orders arising within the CDW phase.

DOI: 10.1103/PhysRevResearch.5.L012017

Kagome materials have recently attracted extensive interest as they offer a unique possibility to investigate both the ground and excited states that emerge from the interplay between a frustrated geometry of the crystalline structure and a nontrivial band topology [1–13]. In this context, the vanadium-based kagome materials AV_3Sb_5 (A = Rb, Cs, K) [14–17] undergo a unique "high-temperature" transition (ranging from $T_{CDW} \in [80–104]$ K) into a charge density wave (CDW) state [15,16,18,19] that precedes and thus hosts both a large anomalous Hall response, and below $T_c \in [0.9–2.5]$ K, unconventional superconductivity [15,16,18,19]. That is to say two of the least microscopically understood phenomena of the contemporary physics develop in the same compound. Furthermore, they are accompanied by other concomitant symmetry-breaking phases, such as chiral order and/or time-reversal symmetry breaking, possibly arising from orbital currents in the CDW state [19–22]. Such symmetry-breaking phases might be responsible for the anomalous Hall effect even in the absence of magnetism of electronic origin [17,23]. A crucial first step to understand the microscopic mechanisms underlying these complex phenomena in the Kagome materials is to decipher the exact order configuration in the CDW. Thus far, the CDW configuration has not been completely assessed. Moreover, previous ARPES+DFT results suggest that the specific CDW structure is cation (Rb, Cs, K) dependent [24], which further complicates the matter.

In this work, we focus on RbV_3Sb_5 and unambiguously identify the ground state structure of the CDW state. We determine that the $2 \times 2 \times 2$ superlattice associated with the CDW structure formed below 103 K is the so-called inverse Star of David pattern, π-shifted along the c axis (also known as staggered trihexagonal).

At room temperature, RbV_3Sb_5 has a layered (henceforth pristine) structure with hexagonal symmetry (space group P6/mmm, No. 191), as shown in Fig. 1(a). It consists of Rb layers and V-Sb slabs alternated along the c axis, and it is isostructural to KV_3Sb_5 and CsV_3Sb_5 [15]. The most important characteristic of this material is the two-dimensional (2D) kagome layer formed by the V atoms [Fig. 1(a)], whose $3d$ orbitals give rise to a number of peculiar features in the electronic band structure [18,25,26]. One of the key features is the occupation of van Hove singularities, possibly dictated by the Sb p-orbitals, close to the Fermi energy [27]. For $T > T_{CDW}$, the high-temperature phase contains two inequivalent Sb sites: Sb1 sites are co-planar with V, while Sb2 sites are located off-plane below and above the V layer. Sb1 sits in the center of V hexagons while Sb2 prospectively falls in the center of V triangles, forming graphenelike hexagon layers.

Below the transition temperature, $T_{CDW} = 103$ K, the lattice undergoes a structural transition into the CDW. Initial, first-principles calculations proposed two possible distortions

*pietro.bonfa@unipr.it
†vesna_mitrovic@brown.edu

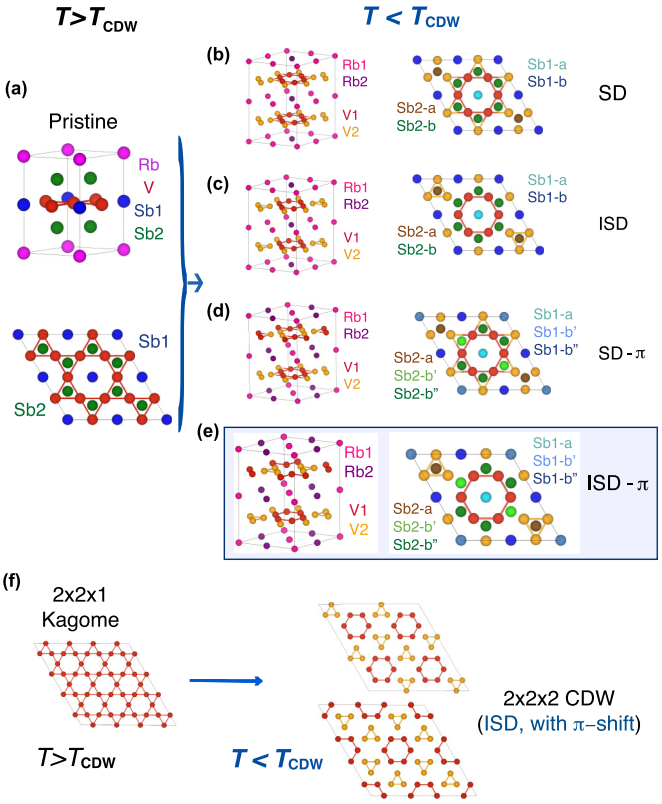

FIG. 1. The crystalline structure of RbV_3Sb_5, above and below the transition temperature into the CDW state (T_{CDW}). (a) The pristine phase adopted above T_{CDW} with the V atoms (in red) forming a 2D kagome lattice. The Sb atoms are divided into two sets: Sb1 (in blue) and Sb2 (in dark green). The Rb atoms are labeled in magenta. [(b)–(e)] The four possible structures proposed below T_{CDW}: Star of David (SD), inverse Star of David (ISD) or trihexagonal, (staggered) Star of David and inverse Star of David with π shift (SD-π and ISD-π, respectively). The Sb atoms in the 3D crystal representation are omitted for clarity. (f) The pattern formed by ^{51}V atoms above and below CDW transition (ISD-π structure), with the formation of V1 and V2 sublattices (colored in red and orange, respectively) in the CDW phase.

for the atomic arrangement in the kagome planes. One is the Star of David (SD) distortion [Fig. 1(b)] of V atoms, which resembles the well-known motif of the CDW state found in transition-metal dichalcogenides [28,29]. The other is an inverse deformation of the SD pattern [ISD, Fig. 1(c)]. This results in a periodic arrangement of the V atoms in triangles and hexagons also referred to as trihexagonal (TrH) structure.

Regarding the stacking along the c axis, different positioning has been proposed: (i) Repetition of SD or ISD [Figs. 1(b) and 1(c)], (ii) alternation of ISD and SD, (iii) a π shift translation between adjacent planes [SD-π and ISD-π, Figs. 1(d) and 1(e)]. Therefore the overall distortion must be described in, at least, a $2 \times 2 \times 2$ supercell space. Higher order modulations have been observed in the Cs variant only, but they manifest in a competing state nearly degenerate with a $2 \times 2 \times 2$ phase.

In Table I, we summarize the currently proposed CDW structures, identified by different techniques for each compound of the AV_3Sb5 (A = Cs, K, Rb) family. Evidently, the assignment of the CDW structure remains highly controversial

TABLE I. Proposed charge-density wave structures ($T < T_{CDW}$) for AV_3Sb5 (A = Cs, K, Rb) from the literature.

	CsV_3Sb_5	KV_3Sb_5	RbV_3Sb_5
ISD-π	N [18,31,32] S [36], D [33,34] X [35,38]	A+D [24,33,34] A [37]	X [35] D [24,33,34]
SD-π	N [18,39], X [35,38] S [36]	/	X [35]
SD+ISD	X [40], A+D [24,41]	A+D [41]	A+D [41]
SD	/	/	/
ISD	/	A [42,43]	A [44]

Legend: N = NMR, X = XRD, S = STM, A = ARPES, D = DFT

and possibly material-dependent. Yet, the identification of the precise CDW configuration and its symmetries is crucial to give the proper basis for the theoretical description of the interplay between these complex charge-ordered states and superconductivity predicted for this family of compounds [30].

In this work, we resolve this controversy for RbV_3Sb_5 by combining ^{51}V / ^{87}Rb NMR and ^{121}Sb NQR measurements with density functional theory (DFT) calculations unambiguously identifying the crystalline structure of the CDW phase as the inverse Star of David pattern π-shifted along the c axis [Figs. 1(e) and 1(f)]. Specifically, ^{51}V / ^{87}Rb nuclear magnetic resonance (NMR) spectral measurements on a single crystal of RbV_3Sb_5 as a function of temperature, in an external magnetic field $B_0 = 7.95$ and 6.99 T, and ^{121}Sb zero-field nuclear quadrupolar resonance (NQR) spectral measurements have been performed. The experimental procedure is detailed in Ref. [45].

The NMR/NQR spectral frequency is sensitive to the local magnetic and charge environment. Therefore nonequivalent nuclear sites arising from the symmetry-breaking effects are typically detected by frequency peak splittings across the phase transition. Therefore NMR and NQR have been demonstrated to be excellent probes allowing to evidence the atomic ordering inside materials [46]. In addition, the area A_i of the ith NMR/NQR spectral peak is proportional to the statistical occupation of a specific ith nuclear site, i.e., to the multiplicity of each nonequivalent site in the unit cell. To obtain the real amplitude for the NMR/NQR peaks, the delays τ between each radio-frequency pulse have been chosen just longer than the receiver dead time but, in all cases, well shorter than the spin-spin relaxation time T_2. We base the determination of the CDW configuration upon the following: (i) The A_i/A_j ratio of the NMR/NQR peaks for each couple of nonequivalent nuclei ($i \neq j$), equal to the population ratio of the nonequivalent nuclear site per species, and (ii) on the quadrupolar frequency ν_Q and asymmetry parameter of the electric field gradient (EFG) tensor η of each peak that we compare to DFT based calculations of the EFG in the various phases.[1]

[1]The detailed description of the computational approach is provided in Ref. [45].

TABLE II. Atomic occupations for ^{51}V , ^{121}Sb , and ^{87}Rb atoms in RbV_3Sb_5 above and below CDW transition.

Phase	Atoms	Multiplicity
Pristine	Rb	1
	V	3
	Sb1	1
	Sb2	4
$2 \times 2 \times 2$ CDW (ISD or SD, no π shift)	Rb1/Rb2	6/2
	V1/V2	12/12
	Sb1-a/Sb1-b	2/6
	Sb2-a/Sb2-b	8/24
$2 \times 2 \times 2$ CDW (ISD or SD, with π shift)	Rb1/Rb2	4/4
	V1/V2	12/12
	Sb1-a/Sb1-b'/Sb1-b"	2/2/4
	Sb2-a/Sb2-b'/Sb2-b"	8/8/16

We find that in the lowest symmetry configurations considered, i.e. SD-π and ISD-π, the V and Rb atoms split into two sublattices, while three nonequivalent sites are obtained for Sb1 and Sb2 nuclei. These configurations are illustrated in Figs. 1(d) and 1(e). The multiplicity of each nonequivalent site is summarized in Table II for both the pristine ($T > T_{CDW}$) and various proposed CDW ($T < T_{CDW}$) phases.

^{121}Sb (with nuclear spin $I = 5/2$) NQR represent the most sensitive measurements enabling distinction between the SD and ISD structures, as shown in the case of CsV_3Sb_5 [31,32]. Due to the different positions and their lower symmetry, Sb2 and Sb1 nuclear sites bifurcate into Sb2-a/Sb2-b and Sb1-a/Sb1-b for the SD or the ISD structures, and further separated into Sb2-a/Sb2-b/Sb2-b" and Sb1-a/Sb1-b'/Sb1-b" nonequivalent sites when a π shift is introduced, as shown in Fig. 1.

In Fig. 2, we present a detailed comparison of magnetic resonance measurements to the DFT simulation results. Specifically, a select set of ^{121}Sb NQR spectra for $5/2 \rightarrow 3/2$ NQR transition is shown. Above $T_{CDW} = 103$ K (bottom of Fig. 2) two peaks are present and assigned according to the 1:4 occupation ratio Sb1:Sb2 [Fig. 1(a) and Table II]. In the CDW phase (center of Fig. 2), we expect four peaks for a simple stacking of SD or ISD-ordered kagome planes, while six peaks should appear when introducing a further π shift along c. The data for $T < T_{CDW}$ show five peaks, with four of them clearly visible and an additional spectral weight appearing as a bump next to the most intense peak. From this, we can exclude the two simpler SD or ISD structures [Figs. 1(b) and 1(c)] with no π shift. This is because these simper structures without a π shift generate only four peaks in the ^{121}Sb NQR spectrum. Moreover, by examining the site multiplicity summarized in Table II, we deduce that the most intense peak, observed in the vicinity of 145 MHz, is assigned to the Sb2-b."

Furthermore, in our ^{121}Sb NQR spectra, we noticed that two peaks have the asymmetry parameter of the EFG $\eta = 0$, in our case Sb2a and Sb1a, by measuring the first and second NQR transitions ($3/2 \rightarrow 1/2$ and $5/2 \rightarrow 3/2$). This is consistent with their lattice positions shown in Fig. 1(e), since their neighbours are symmetrically arranged. In case of an

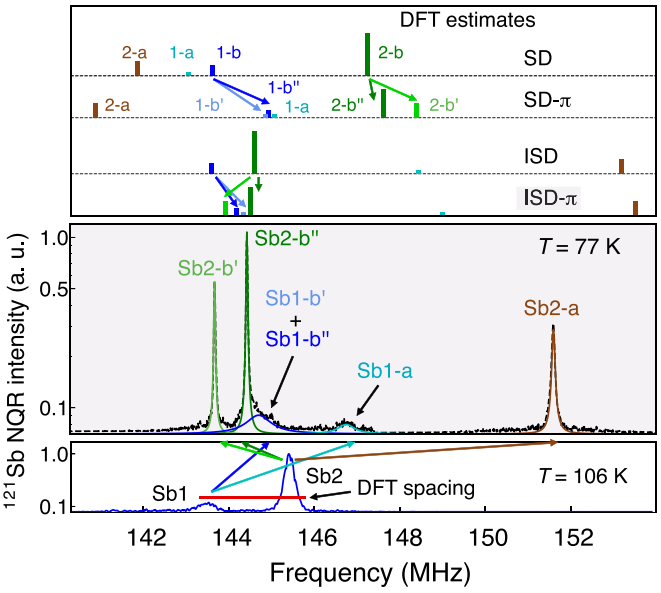

FIG. 2. Representative ^{121}Sb NQR spectra above (106 K, bottom) and below T_{CDW} (77 K, center) for $5/2 \rightarrow 3/2$ NQR transition. In the top part, vertical ticks display the relative values calculated below T_{CDW} by DFT for SD, ISD,, SD-π and ISD-π configurations with respect to the quadrupolar frequency of Sb sites above T_{CDW} (see text); the height of the ticks is proportional to the site multiplicity. In the middle panel, the y scale is logarithmic. In the bottom part, the DFT spacing is calculated for the normal state.

ISD-π CDW structure, Sb2a sites are surrounded by V2 triangles while Sb1a by V1 hexagons; therefore, for these sites, η should be 0, according to their lattice positions. Assuming this, the assignment for all the other ^{121}Sb NQR peaks is straightforward, based on their atomic multiplicity compared to the experimental area of the peaks.

Next, we proceed to estimate the quadrupolar frequencies for the various structures with ab initio simulations by computing the EFG at each ^{121}Sb site in the SD, ISD, SD-π, and ISD-π structures. As detailed in Ref. [45], the absolute values of the calculated ν_Q (i.e., the EFG) at the Sb sites are affected by a systematic error, but canceled when the *variations* of ν_Q between the pristine phase ($T > T_{CDW}$) and the low-temperature structures ($T < T_{CDW}$) are considered. The mismatch between the experimental and the DFT results for the SD structure is clearly evident. That is, Sb2-a and Sb2-b nuclei have very different quadrupolar resonance frequencies for the SD and ISD structures, and therefore the addition of a π shift to the SD structure does not improve the correspondence. However, a good agreement is found instead for the ISD structure and the small change introduced by the π shift along the c direction further improves the agreement between the prediction and experiment. We can therefore rule out the presence of SD distortions in the kagome plane with high fidelity.

We proceed to further compare of our experimental and DFT findings in the ISD-π phase. In Table III, we summarize the A_i/A_j ratio obtained from the area of the NQR peaks and the relative site occupation. The values are in a very good agreement, with the experimental uncertainty. As a result, we

TABLE III. Multiplicity ratio between ^{121}Sb sites in the CDW phase, according to the crystalline structure (center) and experimental NQR area (right column).

Phase	Sites	Crystal	NQR area (T = 77 K)
Pristine	Sb2:Sb1	4	4.20 ± 0.25
CDW	Sb2-b":Sb1-a	8	7.77 ± 0.29
	Sb2-b':Sb1-a	4	4.02 ± 0.17
	Sb2-a:Sb1-a	4	3.87 ± 0.21
	(Sb1-b"+Sb1-b'):Sb1-a	3	3.01 ± 0.18

can attribute the bump in the vicinity of 145 MHz to the combined signal from Sb1-b' and Sb1-b" sites of the π-shifted ISD structure, as shown in the middle, shaded, panel of Fig. 2.

Incidentally, we note that the two peaks at the lowest and highest frequencies have been previously assigned to the Sb1-b and Sb2-a sites by earlier NQR studies [32,39]. However, this conclusion is inconsistent with the expected ratio between the area of the two peaks.

To further justify the site assignment, we also consider the $3/2 \rightarrow 1/2$ NQR transition and estimate the asymmetry parameter η of the EFG tensor from the following ratio, valid if $\eta \leqslant 0.1$ [45,47,48]

$$\frac{\nu_Q^{121}(5/2 \rightarrow 3/2)}{\nu_Q^{121}(3/2 \rightarrow 1/2)} \simeq 2\left(1 - \frac{35}{27}\eta^2\right). \quad (1)$$

The experimental values of η for Sb sites are compared with the DFT prediction for the ISD-π structure in Table IV. Taken together, the above results allow us to unambiguously conclude that the kagome planes in RbV_3Sb_5 undergo an ISD distortion and support the presence of a π shift along c direction, in agreement with recent theoretical predictions [24,33,44].

To further validate the proposed arrangement of the kagome layers along the c axis, we study the symmetry change at the Rb site. In Fig. 3, we plot representative spectra of ^{87}Rb obtained in $H_0 = 7.95$ T field along the c direction. As expected for the quadrupole perturbed NMR spectra of the $I = 3/2$ ^{87}Rb nuclear spin, three peaks appear above T_{CDW} = 103 K, related to the $\pm 1/2$ transition for the central line and the $+3/2 \rightarrow +1/2$ and $-1/2 \rightarrow -3/2$ transitions for the low and high-frequency satellites, respectively. Below T_{CDW} = 103 K, both the satellites and the central line clearly split into additional two peaks each. This splitting indicates the presence of two inequivalent sites, labeled Rb1 and Rb2. We

TABLE IV. Comparison between experimental and predicted values for the asymmetry parameter η.

Site	DFT (ISD-π)	Exp. (T = 77.3 K)
Sb1-a	0	0.001 ± 0.005
Sb1-b'	0.056	0.034 ± 0.005
Sb1-b"	0.058	0.034 ± 0.005
Sb2-a	0	0.001 ± 0.006
Sb2-b'	0.117	0.074 ± 0.006
Sb2-b"	0.116	0.076 ± 0.006

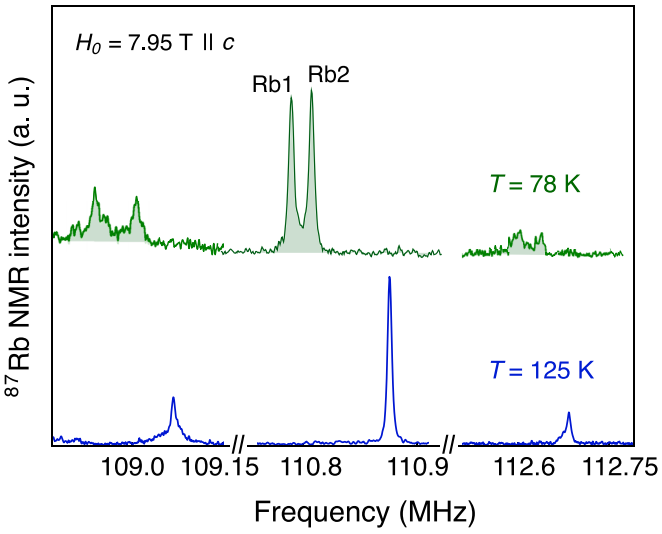

FIG. 3. Temperature dependence of the ^{87}Rb NMR spectra above and below (shaded spectra) $T_{CDW} = 103$ K, with $H_0 = 7.95$ T $\| c$ axis.

observe that 3 ^{87}Rb NMR spectral peaks corresponding to all 3 satellite transitions for the nuclear spin $I = 3/2$ bifurcate below T_{CDW}. This is a direct consequence of different electric field gradients and local susceptibilities at the two sites, as detailed in Ref. [45]. This behavior is in agreement with that observed in the ^{51}V NMR in CsV_3Sb_5 [18,31].

Similar to what was done in the analysis of the ^{121}Sb NQR findings, we consider the relative area between the two NMR peaks of a doublet, which is proportional to the ratio between the multiplicity of the corresponding inequivalent atomic sites. The stacked ISD layer with a π shift [31] yields a 1:1 multiplicity ratio between Rb1 and Rb2 sites. On the other hand, the structures with alternating SD and ISD layers [40] proposed for CsV_3Sb5 and stacks of ISD layers without π shift yield a 3:1 ratio.[2] In Fig. 3, it is evident that the ratio between Rb1 and Rb2 peak intensities is nearly equal to 1:1, either for the central or satellite doublets. This result excludes the alternate SD and ISD configurations. It is rather compatible with the stacking made by only ISD layers π-shifted from one layer to the other.

Finally, our ^{51}V NMR results are in agreement with those published for A = Cs [18,31,32] despite the difference in the spacing layer. Moreover, since the V1:V2 occupation ratio is predicted to be 1:1 for both the SD and ISD structures, ^{51}V NMR is an inadequate probe for identifying the CDW configuration in the kagome plane. These ^{51}V results are reported in Ref. [45].

In conclusion, we measured a comprehensive set of NMR spectra, that include zero-field ^{121}Sb, and, finite field ^{51}V and ^{87}Rb. The analysis of the NMR/NQR spectra from all three nuclear species, substantiated by DFT simulations, lead to an unambiguous identification of the structure stabilized below the CDW transition. Specifically, the examination of

[2]The comparison among different structures can be seen in Supplementary materials of Ref. [31].

the multiplicity of the nonequivalent sites for each species revealed that the low-temperature structure is a $2 \times 2 \times 2$ superlattice formed by alternating inverse Star of David layers, π-shifted from one to the other. This result provides crucial guidance for the development of theoretical models of the complex emergent phases stabilized in the kagome metals.

Note added. Recently, we became aware of a new preprint that reaches similar conclusions for CsV_3Sb_5 using a very similar methodology [49].

Work at Brown was supported in part by the US National Science Foundation (NSF) Grant No. DMR-1905532 and funds from Brown and the University of Bologna. S.D.W. and B.R.O. gratefully acknowledge support via the UC Santa Barbara NSF Quantum Foundry funded via the Q-AMASE-i program under award DMR-1906325. G.A., P.B., and R.D.R. acknowledge support from the University of Parma, under Bando Attrezzature 2020, HyReSpect-4 project. P.B. and R.D.R. acknowledge funding from the SUPER (Supercomputing Unified Platform - Emilia-Romagna) regional project, the National Recovery and Resilience Plan (NRRP), Mission 04 Component 2 Investment 1.5 NextGenerationEU, Call for tender No. 3277, 30/12/2021 Award 0001052, 23/06/2022 computing power form STFC's SCARF cluster and CINECA (ISCRA-C Grant No. HP10CZHPHI).

[1] S. Depenbrock, I. P. McCulloch, and U. Schollwöck, Nature of the Spin-Liquid Ground State of the $S = 1/2$ Heisenberg Model on the Kagome Lattice, Phys. Rev. Lett. **109**, 067201 (2012).

[2] N. Ghimire and I. Mazin, Topology and correlations on the kagome lattice, Nat. Mater. **19**, 137 (2020).

[3] D. A. Huse and A. D. Rutenberg, Classical antiferromagnets on the Kagome lattice, Phys. Rev. B **45**, 7536 (1992).

[4] A. Kitaev, Anyons in an exactly solved model and beyond, Ann. Phys. **321**, 2 (2006).

[5] W. Koshibae and S. Maekawa, Electronic State of a CoO_2 Layer with Hexagonal Structure: A Kagome Lattice Structure in a Triangular Lattice, Phys. Rev. Lett. **91**, 257003 (2003).

[6] Z. Li, J. Zhuang, L. Wang, H. Feng, Q. Gao, X. Xu, W. Hao, X. Wang, C. Zhang, K. Wu, S. X. Dou, L. Chen, Z. Hu, and Y. Du, Realization of flat band with possible nontrivial topology in electronic Kagome lattice, Sci. Adv. **4**, eaau4511 (2018).

[7] K. Morita, M. Kishimoto, and T. Tohyama, Ground-state phase diagram of the Kitaev-Heisenberg model on a kagome lattice, Phys. Rev. B **98**, 134437 (2018).

[8] R. R. P. Singh and D. A. Huse, Triplet and singlet excitations in the valence bond crystal phase of the kagome lattice Heisenberg model, Phys. Rev. B **77**, 144415 (2008).

[9] M. Taillefumier, J. Robert, C. L. Henley, R. Moessner, and B. Canals, Semiclassical spin dynamics of the antiferromagnetic Heisenberg model on the kagome lattice, Phys. Rev. B **90**, 064419 (2014).

[10] M. G. Yamada, T. Soejima, N. Tsuji, D. Hirai, M. Dincă, and H. Aoki, First-principles design of a half-filled flat band of the kagome lattice in two-dimensional metal-organic frameworks, Phys. Rev. B **94**, 081102(R) (2016).

[11] M. L. Kiesel, C. Platt, and R. Thomale, Unconventional Fermi Surface Instabilities in the Kagome Hubbard Model, Phys. Rev. Lett. **110**, 126405 (2013).

[12] W.-S. Wang, Z.-Z. Li, Y.-Y. Xiang, and Q.-H. Wang, Competing electronic orders on kagome lattices at van Hove filling, Phys. Rev. B **87**, 115135 (2013).

[13] S.-L. Yu and J.-X. Li, Chiral superconducting phase and chiral spin-density-wave phase in a Hubbard model on the kagome lattice, Phys. Rev. B **85**, 144402 (2012).

[14] Y. Wang, S. Yang, P. K. Sivakumar, B. R. Ortiz, S. M. L. Teicher, H. Wu, A. K. Srivastava, C. Garg, D. Liu, S. S. P. Parkin, E. S. Toberer, T. McQueen, S. D. Wilson, and M. N. Ali, Proximity-induced spin-triplet superconductivity and edge supercurrent in the topological Kagome metal, $K_{1-x}V_3Sb_5$, arXiv:2012.05898.

[15] B. R. Ortiz, L. C. Gomes, J. R. Morey, M. Winiarski, M. Bordelon, J. S. Mangum, I. W. H. Oswald, J. A. Rodriguez-Rivera, J. R. Neilson, S. D. Wilson, E. Ertekin, T. M. McQueen, and E. S. Toberer, New kagome prototype materials: Discovery of KV_3Sb_5, RbV_3Sb_5, and CsV_3Sb_5, Phys. Rev. Mater. **3**, 094407 (2019).

[16] B. R. Ortiz, S. M. L. Teicher, Y. Hu, J. L. Zuo, P. M. Sarte, E. C. Schueller, A. M. M. Abeykoon, M. J. Krogstad, S. Rosenkranz, R. Osborn, R. Seshadri, L. Balents, J. He, and S. D. Wilson, CsV_3Sb_5: A $\mathbb{Z}_2$ Topological Kagome Metal with a Superconducting Ground State, Phys. Rev. Lett. **125**, 247002 (2020).

[17] S.-Y. Yang, Y. Wang, B. R. Ortiz, D. Liu, J. Gayles, E. Derunova, R. Gonzalez-Hernandez, L. Šmejkal, Y. Chen, S. S. P. Parkin, S. D. Wilson, E. S. Toberer, T. McQueen, and M. N. Ali, Giant, unconventional anomalous Hall effect in the metallic frustrated magnet candidate, KV_3Sb_5, Sci. Adv. **6**, eabb6003 (2020).

[18] D. W. Song, L. X. Zheng, F. H. Yu, J. Li, L. P. Nie, M. Shan, D. Zhao, S. J. Li, B. L. Kang, Z. M. Wu, Y. B. Zhou, K. L. Sun, K. Liu, X. G. Luo, Z. Y. Wang, J. J. Ying, X. G. Wan, T. Wu, and X. H. Chen, Orbital ordering and fluctuations in a kagome superconductor CsV_3Sb_5, Sci. China Phys. Mech. Astron. **65**, 247462 (2022).

[19] N. Shumiya, M. S. Hossain, J.-X. Yin, Y.-X. Jiang, B. R. Ortiz, H. Liu, Y. Shi, Q. Yin, H. Lei, S. S. Zhang, G. Chang, Q. Zhang, T. A. Cochran, D. Multer, M. Litskevich, Z.-J. Cheng, X. P. Yang, Z. Guguchia, S. D. Wilson, and M. Z. Hasan, Intrinsic nature of chiral charge order in the kagome superconductor RbV_3Sb_5, Phys. Rev. B **104**, 035131 (2021).

[20] Y. Jiang *et al.*, Unconventional chiral charge order in kagome superconductor KV_3Sb_5, Nat. Mater. **20**, 1353 (2021).

[21] Y. M. Oey, B. R. Ortiz, F. Kaboudvand, J. Frassineti, E. Garcia, R. Cong, S. Sanna, V. F. Mitrovic, R. Seshadri, and S. D. Wilson, Fermi level tuning and double-dome superconductivity in the kagome metal $CsV_3Sb_{5-x}Sn_x$, Phys. Rev. Mater. **6**, L041801 (2022).

[22] C. Mielke III, D. Das, J.-X. Yin, H. Liu, R. Gupta, Y.-X. Jiang, M. Medarde, X. Wu, H. C. Lei, J. Chang, P. Dai, Q. Si, H. Miao, R. Thomale, T. Neupert, Y. Shi, R. Khasanov, M. Z. Hasan, H. Luetkens, and Z. Guguchia, Time-reversal symmetry-breaking

charge order in a kagome superconductor, Nature **602**, 245 (2022).

[23] E. M. Kenney, B. R. Ortiz, C. Wang, S. D. Wilson, and M. J. Graf, Absence of local moments in the kagome metal KV_3Sb_5 as determined by muon spin spectroscopy, J. Phys.: Condens. Matter **33**, 235801 (2021).

[24] M. Kang, S. Fang, J. Yoo, B. R. Ortiz, Y. Oey, J. Choi, S. H. Ryu, J. Kim, C. Jozwiak, A. Bostwick, E. Rotenberg, E. Kaxiras, J. Checkelsky, S. D. Wilson, J.-H. Park, and R. Comin, Charge order landscape and competition with superconductivity in kagome metals, Nature Materials **22**, 186 (2023).

[25] Y. Hu, X. Wu, B. R. Ortiz, S. Ju, X. Han, J. Ma, N. C. Plumb, M. Radovic, R. Thomale, S. D. Wilson, A. P. Schnyder, and M. Shi, Rich nature of Van Hove singularities in Kagome superconductor CsV_3Sb_5, Nat. Commun. **13**, 2220 (2022).

[26] A. Consiglio, T. Schwemmer, X. Wu, W. Hanke, T. Neupert, R. Thomale, G. Sangiovanni, and D. Di Sante, Van hove tuning of AV_3Sb_5 kagome metals under pressure and strain, Phys. Rev. B **105**, 165146 (2022).

[27] M. Y. Jeong, H.-J. Yang, H. S. Kim, Y. B. Kim, S. B. Lee, and M. J. Han, Crucial role of out-of-plane Sb p orbitals in Van Hove singularity formation and electronic correlations in the superconducting kagome metal CsV_3Sb_5, Phys. Rev. B **105**, 235145 (2022).

[28] J. Wilson, F. D. Salvo, and S. Mahajan, Charge-density waves and superlattices in the metallic layered transition metal dichalcogenides, Adv. Phys. **24**, 117 (1975).

[29] K. Rossnagel, On the origin of charge-density waves in select layered transition-metal dichalcogenides, J. Phys.: Condens. Matter **23**, 213001 (2011).

[30] M. H. Christensen, T. Birol, B. M. Andersen, and R. M. Fernandes, Loop currents in AV_3Sb_5 kagome metals: Multipolar and toroidal magnetic orders, Phys. Rev. B **106**, 144504 (2022).

[31] L. Nie, K. Sun, W. Ma, D. Song, L. Zheng, Z. Liang, P. Wu, F. Yu, J. Li, M. Shan, D. Zhao, S. Li, B. Kang, Z. Wu, Y. Zhou, K. Liu, Z. Xiang, J. Ying, Z. Wang, T. Wu *et al.*, Charge-density-wave-driven electronic nematicity in a kagome superconductor, Nature **604**, 59 (2022).

[32] C. Mu, Q. Yin, Z. Tu, C. Gong, P. Zheng, H. Lei, Z. Li, and J. Luo, Tri-hexagonal charge order in kagome metal CsV_3Sb_5 revealed by ^{121}Sb nuclear quadrupole resonance, Chin. Phys. B **31**, 017105 (2022).

[33] H. Tan, Y. Liu, Z. Wang, and B. Yan, Charge Density Waves and Electronic Properties of Superconducting Kagome Metals, Phys. Rev. Lett. **127**, 046401 (2021).

[34] A. Ptok, A. Kobiałka, M. Sternik, J. Łażewski, P. T. Jochym, A. M. Oleś, and P. Piekarz, Dynamical study of the origin of the charge density wave in AV_3Sb_5 (A = K, Rb, Cs) compounds, Phys. Rev. B **105**, 235134 (2022).

[35] H. Li, T. T. Zhang, T. Yilmaz, Y. Y. Pai, C. E. Marvinney, A. Said, Q. W. Yin, C. S. Gong, Z. J. Tu, E. Vescovo, C. S. Nelson, R. G. Moore, S. Murakami, H. C. Lei, H. N. Lee, B. J. Lawrie, and H. Miao, Observation of Unconventional Charge Density Wave without Acoustic Phonon Anomaly in Kagome Superconductors AV_3Sb_5 (A = Rb, Cs), Phys. Rev. X **11**, 031050 (2021).

[36] Z. Liang, X. Hou, F. Zhang, W. Ma, P. Wu, Z. Zhang, F. Yu, J.-J. Ying, K. Jiang, L. Shan, Z. Wang, and X.-H. Chen, Three-Dimensional Charge Density Wave and Surface-Dependent Vortex-Core States in a Kagome Superconductor CsV_3Sb_5, Phys. Rev. X **11**, 031026 (2021).

[37] Z. Jiang, H. Ma, W. Xia, Q. Xiao, Z. Liu, Z. Liu, Y. Yang, J. Ding, Z. Huang, J. Liu, Y. Qiao, J. Liu, Y. Peng, S. Cho, Y. Guo, J. Liu, and D. Shen, Observation of electronic nematicity driven by three-dimensional charge density wave in kagome lattice KV_3Sb_5, arXiv:2208.01499.

[38] Q. Stahl, D. Chen, T. Ritschel, C. Shekhar, E. Sadrollahi, M. C. Rahn, O. Ivashko, M. v. Zimmermann, C. Felser, and J. Geck, Temperature-driven reorganization of electronic order in CsV_3Sb_5, Phys. Rev. B **105**, 195136 (2022).

[39] J. Luo, Z. Zhao, Y. Z. Zhou, J. Yang, A. F. Fang, H. T. Yang, H. J. Gao, R. Zhou, and G.-q. Zheng, Possible Star-of-David pattern charge density wave with additional modulation in the kagome superconductor CsV_3Sb_5, npj Quantum Mater. **7**, 30 (2022).

[40] B. R. Ortiz, S. M. L. Teicher, L. Kautzsch, P. M. Sarte, N. Ratcliff, J. Harter, J. P. C. Ruff, R. Seshadri, and S. D. Wilson, Fermi Surface Mapping and the Nature of Charge-Density-Wave Order in the Kagome Superconductor CsV_3Sb_5, Phys. Rev. X **11**, 041030 (2021).

[41] Y. Hu, X. Wu, B. R. Ortiz, X. Han, N. C. Plumb, S. D. Wilson, A. P. Schnyder, and M. Shi, Coexistence of trihexagonal and star-of-David pattern in the charge density wave of the kagome superconductor AV_3Sb_5, Phys. Rev. B **106**, L241106 (2022).

[42] H. Luo, Q. Gao, H. Liu, Y. Gu, D. Wu, C. Yi, J. Jia, S. Wu, X. Luo, Y. Xu, L. Zhao, Q. Wang, H. Mao, G. Liu, Z. Zhu, Y. Shi, K. Jiang, J. Hu, Z. Xu, and X. J. Zhou, Electronic nature of charge density wave and electron-phonon coupling in kagome superconductor KV_3Sb_5, Nat. Commun. **13**, 273 (2022).

[43] T. Kato, Y. Li, T. Kawakami, M. Liu, K. Nakayama, Z. Wang, A. Moriya, K. Tanaka, T. Takahashi, Y. Yao, and T. Sato, Three-dimensional energy gap and origin of charge-density wave in kagome superconductor KV_3Sb_5, Commun. Mater. **3**, 30 (2022).

[44] S. Cho, H. Ma, W. Xia, Y. Yang, Z. Liu, Z. Huang, Z. Jiang, X. Lu, J. Liu, Z. Liu, J. Li, J. Wang, Y. Liu, J. Jia, Y. Guo, J. Liu, and D. Shen, Emergence of New van Hove Singularities in the Charge Density Wave State of a Topological Kagome Metal RbV_3Sb_5, Phys. Rev. Lett. **127**, 236401 (2021).

[45] See Supplemental Material at http://link.aps.org/supplemental/10.1103/PhysRevResearch.5.L012017 for NMR/NQR methods on RbV_3Sb_5 single crystal and computational details, which includes Refs. [16,33,47,48,50–60].

[46] I. R. Mukhamedshin, A. V. Dooglav, S. A. Krivenko, and H. Alloul, Evolution of Co charge disproportionation with Na order in Na_xCoO_2, Phys. Rev. B **90**, 115151 (2014).

[47] A. Abragam, *The Principles of Nuclear Magnetism* (Oxford University Press, 1983).

[48] T. P. Das and E. L. Hahn, *Nuclear Quadrupole Resonance Spectroscopy* (American Institute of Physics, 1959).

[49] Y. Wang, T. Wu, Z. Li, K. Jiang, and J. Hu, The structure of kagome superconductors av_3sb_5 in the charge density wave states, arXiv:2210.07585.

[50] Q. Yin, Z. Tu, C. Gong, Y. Fu, S. Yan, and H. Lei, Superconductivity and normal-state properties of kagome metal RbV_3Sb_5 single crystals, Chin. Phys. Lett. **38**, 037403 (2021).

[51] W. G. Clark, M. E. Hanson, and F. Lefloch, Magnetic resonance spectral reconstruction using frequency-shifted and summed

Fourier transform processing, Rev. Sci. Instrum. **66**, 2453 (1995).
[52] ELK code v8.3.25.
[53] M. Methfessel and A. T. Paxton, High-precision sampling for Brillouin-zone integration in metals, Phys. Rev. B **40**, 3616 (1989).
[54] J. P. Perdew, K. Burke, and M. Ernzerhof, Generalized Gradient Approximation Made Simple, Phys. Rev. Lett. **77**, 3865 (1996).
[55] H. J. Monkhorst and J. D. Pack, Special points for Brillouin-zone integrations, Phys. Rev. B **13**, 5188 (1976).
[56] J. D. Pack and H. J. Monkhorst, "Special points for Brillouin-zone integrations"— a reply, Phys. Rev. B **16**, 1748 (1977).
[57] G. Allodi, A. Banderini, R. D. Renzi, and C. Vignali, HyReSpect: A broadband fast-averaging spectrometer for nuclear magnetic resonance of magnetic materials, Rev. Sci. Instrum. **76**, 083911 (2005).
[58] E. L. Hahn, Spin echoes, Phys. Rev. **80**, 580 (1950).
[59] D. M. S. Bagguley, *Pulsed Magnetic Resonance - NMR, ESR, and Optics: A Recognition of E. L. Hahn* (Oxford University Press, 1992).
[60] R. E. Wasylishen, *NMR Of Quadrupolar Nuclei In Solid Materials* (Wiley, 2012).